Bottom-Up Synthesized Graphene Nanoribbon Transistors

Zafer Mutlu and Jeffrey Bokor

EECS Department, University of California, Berkeley, CA, USA, zmutlu@berkeley.edu

Abstract

Bottom-up synthesized graphene nanoribbons (GNRs) exhibit promising electronic properties for post-silicon transistor technologies. However, several challenges remain, such as the synthesis of long length GNRs, their rational placement and alignment on dielectric surface, and achieving low GNR-contacts and uniform high- κ gate dielectrics. This invited talk presents recent progress in integrating GNRs into field-effect transistors (FETs) and discusses the synthesis and integration improvements that may enable the fabrication of GNR devices with the performance needed for the post-silicon era.

Keywords: Transistors and graphene nanoribbons

Introduction

Recent advances in on-surface organic synthesis have led to the development of rational bottom-up GNR growth with atomic precision [1]. This atomic precision leads to versatile electronic properties tailored by the widths and edge topologies, which make GNRs promising candidates for future transistor technologies and quantum information processing [2]. However, a range of fundamental synthesis, integration, and device engineering challenges have impeded the fabrication of devices with the expected performance [3]. Here, recent progress in integrating GNRs into devices is presented. GNRFETs with a nine-atom wide armchair GNRs (9-AGNRs) exhibit high on-state current (ION) and excellent on/off current ratio (I_{ON}/I_{OFF}) [4, 5]. The impact of GNR length, channel length (L) and channel width (W) on the ION and I_{ON}/I_{OFF} are studied. Atomic layer deposition (ALD) of uniform high-k top gate (TG) dielectric layer atop GNRs has been demonstrated [5]. Finally, a novel highly scalable method [6] for transfer-free fabrication of GNRFETs has been developed.

Results and Discussion

The first step in the fabrication of 9-AGNRFETs entails the bottom-up synthesis of the GNRs on the surface of a Au(111)/mica substrate from the iodine (I)- or bromine (Br)-based precursor. [7] For simplicity, by depending on the precursor used for their growth, the GNRs are denoted by 9-AGNR (I) or 9-AGNR (Br). As shown in Fig. 1a, the reaction

proceeds via two steps ($T_1 = 200 \, ^{\circ}\text{C}$ and $T_2 = 400 \, ^{\circ}\text{C}$), involving polymerization and cyclodehydrogenation (CDH). In Fig. 1b, the STM imaging reveals that 9GNRs (I) are uniform, straight, and densely packed. The GNRs are wet transferred onto a pre-patterned SiO2/Si chip containing local back gate (BG) devices with W gate metal capped with 5.5 nm HfO2 ALD dielectric layer (equivalent oxide thickness, EOT = ~1.8 nm, dielectric capacitance, $C_{ox} = ~19.0 \,\mu\text{F/cm}^2$). Raman spectroscopy measurements are taken on 9-AGNRs before and after transfer, shown in Fig. 1c. The presence of the characteristic RBLM, C-H, D, and G modes confirms the successful growth and transfer of the GNRs. After transfer, the GNRs are contacted with 12 nm thick Pd electrodes, with 20-65 nm gaps defining L and 30-200 nm electrode widths defining W, by electron beam lithography (See [8] for the details of transfer and device fabrication). Fig. 1d and 1e shows cross-sectional diagram and SEM image of a BG 9-AGNRFET, respectively.

Typical transport characteristics of a 9-AGNRFET measured at room temperature under high vacuum (<10⁻⁵ torr) are shown in Fig. 2a and 2b. The transfer characteristic (drain current (I_D) vs. gate voltage (V_{GS}) exhibits a p-type FET behavior with a high I_{ON} of ~1 μ A at a fixed drain voltage (V_{DS}) of -1 V, and an excellent ION/IOFF of 10⁵, shown in Fig. 2a. The super-linearity of the output characteristics (I_D vs. V_{DS}) indicates tunneling transport through of a finite Schottky barrier (SB) at the GNR-Pd interface, shown in Fig. 2b. The Ion of 9-AGNRFET is at least 10 times higher than the best reported values for seven atom wide AGNR (7-AGNR) FETs [6,9]. Theoretically predicted bandgaps of freestanding 9-AGNR and 7-AGNR are 2.29 eV and 3.79 eV, respectively [10]. The smaller band gap of 9-AGNR reduces the SB height, leading to the higher Ion [4]. As shown in Fig. 2c, the Ion of 9-AGNR (I)-FETs is also much higher than that of 9-AGNR (Br)-FETs [4]. This could be explained by the larger number of GNRs bridging the source-drain (SD) gap thanks to the much longer lengths of the GNRs grown from the I-based precursor [7].

Fig. 2d shows the L dependence of the $I_{\rm ON}$ and $I_{\rm ON}/I_{\rm OFF}$ for the same W. The $I_{\rm ON}$ increases as the L is downscaled. The increased $I_{\rm ON}$ with the decreased L can be explained by the larger number of connected GNRs and longer contact length (L_c) of the GNR-Pd

interfaces. The $I_{\rm ON}/I_{\rm OFF}$ also increases with the decreased L. However, below L=40 nm, the I_{ON}/I_{OFF} , and subthreshold swing (SS) (not shown) decreases exponentially, due to a fast degradation of the gate control over GNR channel. The dramatic degradation of the gate control at such L scale is not expected for an ideal GNR channel on a 5.5 nm thick HfO2 gate dielectric [11]. Degradation of the SS can be partially explained by possible GNR-GNR screening and bundling effects that cause a weakened gate coupling efficiency and higher effective body thickness, respectively. The dependence of the I_{ON} with the Wfor the same L is also studied. Fig. 2e shows the $I_{\rm ON}$ distributions for the different W. While the median values of the $I_{\rm ON}$ for different W still shows some dependence, it is difficult to accurately quantify the relationship due to the large device-to-device variation. The variations are likely due to variations in the L_c of the GNR-Pd interface, the number of GNRs bridging the channel, the electrode edge roughness, and gate dielectric uniformity.

A dual gate (DG) device with both TG and BG with high- κ dielectric should provide improved electrostatic control over GNR channel, leading to improved $I_{\rm ON}/I_{\rm OFF}$ and SS. To verify this, 1–1.25 nm Al₂O₃ was deposited as a conformal seeding layer at 50 °C using TMA and H₂O directly atop BG devices, followed by 2.5 nm HfO₂ ALD using TDMAH and H₂O at 200 °C. Fig. 2f shows the cumulative distribution of the SS for BG and DG 9-AGNR devices. While no improvement is observed in the $I_{\rm ON}$, TG fabrication results in improved SS and low hysteresis owing to its superior electrostatic control.

Finally, a new method for the transfer-free placement of GNRs on insulators has been demonstrated. This involves growing GNRs on a gold film deposited onto an insulating layer followed by gentle wet etching of the gold, which allows the nanoribbons to settle in place on the underlying insulating substrate, as shown in Fig. 3. The method can scale up well to 12 in. wafers, which is extremely difficult for previous transfer techniques.

Conclusion

In conclusion, BG and DG short-channel GNR FETs with excellent switching behavior and on-state performance have been demonstrated. The influence of GNR length, channel length and width, and TG dielectric on the device performance revealed by this study elucidates the need to further increase GNR

length, to develop methods for deterministic placement of GNR arrays, reduce GNR-GNR screening and bundling effects, and to improve the metal-GNR contact. Efforts in these directions are currently in progress.

Acknowledgments

Work was supported in part by ONR MURI N00014-16-1-2921, NSF E³S Center, and NSF DMR-1839098, Berkeley BETR Center, and TSMC JDP. Work was performed partially at Stanford SNSF (NSF ECCS-1542152) and LBNL Molecular Foundry (DE-AC02-05CH11231). Z.M. thanks G. B. Barin and P. H. Jacobse for STM imaging and artwork, respectively.

References

- [1] J. Cai et al, Atomically Precise Bottom-up Fabrication of Graphene Nanoribbons, *Nature*, 466, 470 (2010).
- [2] H. Wang et al., Graphene Nanoribbons for Quantum Electronics, *Nat. Rev. Phys.* (2021).
- [3] V. Saraswat et al., Materials Science Challenges to Graphene Nanoribbon Electronics, *ACS Nano*, 15, 3674 (2021).
- [4] J. P. Llinas et al., Short-Channel Field-Effect Transistors with 9-Atom and 13-Atom Wide Graphene Nanoribbons, *Nat. Commun.*, 8, 633 (2017).
- [5] Z. Mutlu et al., Short-Channel Double-Gate FETs with Atomically Precise Graphene Nanoribbons, presented at *IEDM* (2021).
- [6] Z. Mutlu et al., Transfer-Free Synthesis of Atomically Precise Graphene Nanoribbons on Insulating Substrates, *ACS Nano*, 15, 2635 (2021).
- [7] M. Di Giovannantonio et al., On-Surface Growth Dynamics of Graphene Nanoribbons: The Role of Halogen Functionalization, *ACS Nano*, 12, 74 (2021).
- [8] Z. Mutlu et al., Bottom-Up Synthesized Nanoporous Graphene Transistors, *Adv. Funct. Mater.* 2103798 (2021).
- [9] P. B. Bennett et al., Bottom-Up Graphene Nanoribbon Field-Effect Transistors, *Appl. Phys. Lett.* 103, 253114 (2013).
- [10] O. Deniz et al., Revealing the Electronic Structure of Silicon Intercalated Armchair Graphene Nanoribbons by Scanning Tunneling Spectroscopy, *Nano Lett.* 17, 2197(2017).
- [11] C. -S. Lee et al, A Compact Virtual-Source Model for Carbon Nanotube FETs in the Sub-10-nm Regime-Part I: Intrinsic Elements, *IEEE Trans. Electron Devices*, 62, 3061 (2015).

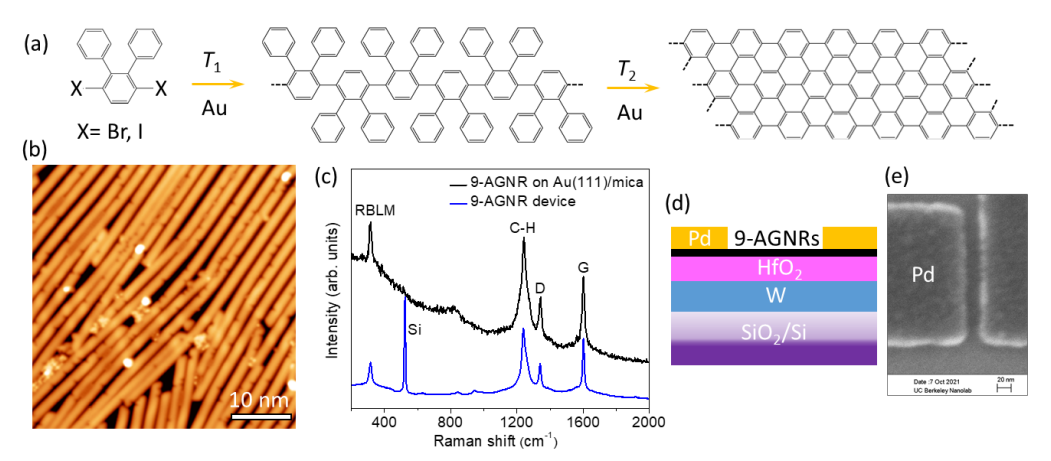


Fig. 1: (a) Reaction path for the growth of 9-AGNRs. (b) STM of 9-AGNRs (I) on Au(111)/mica (c) Raman spectra of 9-AGNRs (I) on Au(111)/mica and device (collected with 785 nm wavelength laser excitation). Cross-sectional diagram (d) and SEM image (e) of BG 9-AGNRFET.

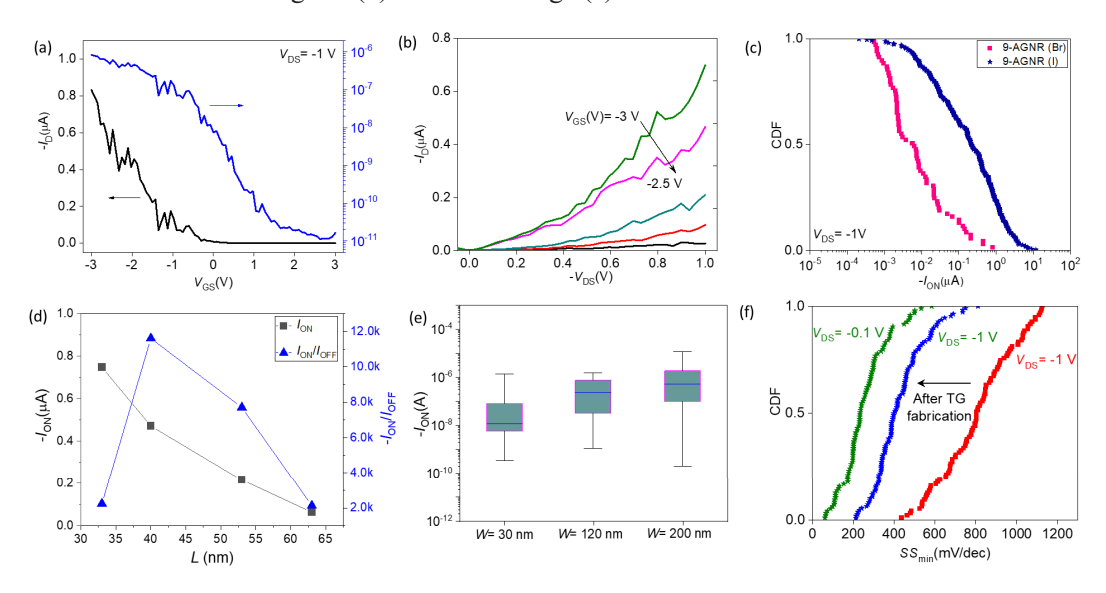


Fig. 2: (a) I_D – V_{GS} characteristic of 9-AGNRFET in linear scale (left axis) and in logarithmic scale (right axis). (b) I_D – V_{DS} characteristic of the same device with varying V_{GS} . (c) Cumulative distribution function (CDF) of the I_{ON} for the FETs with the 9-AGNRs (Br) (>50 devices) and 9-AGNRs (I) (>100 devices). (d) The median I_{ON} of the 9-AGNRFETs with W = 200 nm and different L (>30 devices for each L). (e) The median I_{ON} of the 9-AGNRFETs with L = 40 nm with different W (>30 devices for each W). The blue line corresponds to the median current, while the box bounds 25 and 75 percentiles with whiskers at 1 and 99 percentiles. (f) CDF of the SS before and after TG fabrication.

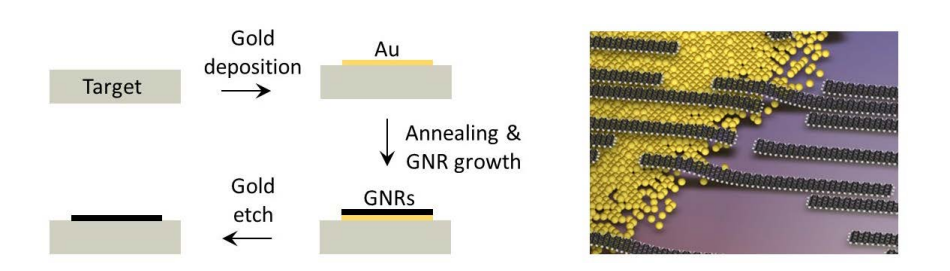


Fig. 3: Schematic illustration of the transfer-free synthesis of GNRs on an insulating target substrate.